OPEN ACCESS
IOP Publishing
Journal of Optics
J. Opt. **27** (2025) 043003 (15pp)
https://doi.org/10.1088/2040-8986/adb85f

Topical Review

Propagation of optical pulses in a spatiotemporal dispersive medium

Govind P Agrawal

The Institute of Optics, University of Rochester, Rochester, NY 14627, United States of America

E-mail: govind.agrawal@rochester.edu

Received 24 October 2024, revised 6 February 2025
Accepted for publication 20 February 2025
Published 28 February 2025

Abstract

This review focuses on novel phenomena that emerge when optical pulses propagate through a spatiotemporal dispersive medium whose refractive index is modulated, both in space and time, in a traveling-wave fashion. Using optical fibers as an example of a dispersive medium, we first derive an equation governing the evolution of short pulses in such a medium. This equation is used to discuss the phenomena such as temporal reflection and refraction, total internal reflection, and waveguiding from a moving boundary with different refractive indices on its two sides. The use of solitons, forming through the Kerr effect, shows how such effects can be observed with silica fibers by employing a pump-probe configuration. A pair of solitons provide the temporal analog of a waveguide or a Fabry–Perot resonator. A new kind of grating, called a spatiotemporal Bragg grating, is formed when a train of pump pulses creates periodic high-index regions inside an optical fiber moving at the speed of pump pulses. The interaction of probe pulses with such a Bragg grating is studied both within and outside of momentum gaps. It is also shown that a photonic analog of Anderson localization is possible when disorder is introduced into a spatiotemporal Bragg grating.

Keywords: optical fibers, nonlinear optics, optical waveguides, temporal reflection

1. Introduction

The concept of space-time duality in optics, noticed in the 1960s [1, 2], has led to many advances in recent years [3]. Noteworthy among these are phenomena such as imaging with a time lens [4], single-shot spectroscopy based on dispersive Fourier transform [5], and temporal analogs of reflection and refraction [6–8]. Considerable attention has been paid recently to wave propagation in a medium whose refractive index (or electric permittivity) varies with time [9–14], although such a medium was studied as early as 1958 [15].

In most studies, refractive index of the time-varying medium is taken to be modulated in time in a spatially uniform fashion on the time scale of a single cycle of the optical field incident on it. By changing the medium's refractive index in a periodic fashion, it is even possible to form a photonic time crystal [16–18]. As it is difficult to produce rapid index changes all across a medium on femtosecond time scales, experiments have involved low frequencies using water waves [19], microwaves [20], or ultra-cold atoms [21]. Further, effects of chromatic dispersion, neglected in most theoretical studies, should be considered for any dielectric medium with a time-varying refractive index.

It turns out that these issues can be addressed with the technique of traveling-wave modulation, which changes the refractive index of a dispersive medium in a region that moves

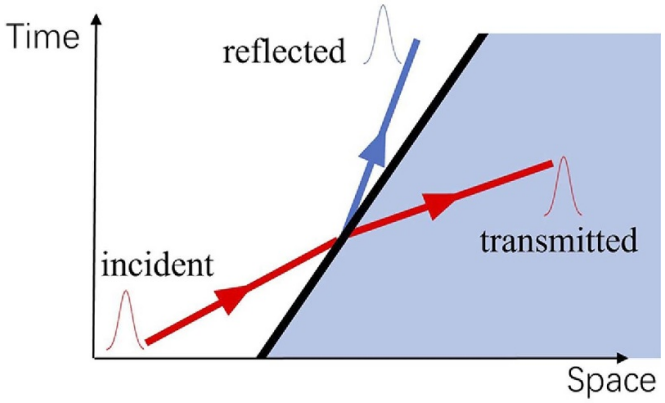

Figure 1. Temporal analogs of reflection and refraction at a temporal boundary (tilted black line) with different refractive indices on its two sides. Arrows indicate the incident, reflected, and transmitted waves.

at a constant speed [8, 10, 22]. Since refractive index in this situation varies both in space and time, we refer to the medium as a spatiotemporal dispersive medium. The simplest case, shown schematically in figure 1, corresponds to a moving boundary (thick black line) with different refractive indices on its two sides. When an optical pulse interacts with this boundary inside a dispersive medium, it splits into two parts, whose frequencies are shifted such that they travel at different speeds [23–26]. These two parts correspond to transmitted and reflected pulses and are temporal analogs of the reflection and refraction at a spatial interface [8]. This type of temporal reflection does not require index modulation to occur on a single-cycle time scale. Further, it is possible to realize a temporal analog of total internal reflection and to use it for temporal waveguiding [23]. In this review, I focus on a spatiotemporal dispersive medium and discuss how it can be used for observing several interesting phenomena.

A moving index boundary can be realized using the optical Kerr effect. In this case, intense pump pulses are launched into a nonlinear dispersive medium, such as an optical fiber. The fiber's local refractive index increases in a time window set by the width of pump pulses [27], and this window moves at the speed of pump pulses. When a probe pulse, moving at a different speed because of its different wavelength, interacts with this index window, a reflected pulse is generated at a wavelength shifted from that of the probe [24]. A pump-probe configuration has been considered in the field of *nonlinear fiber optics* in many different contexts [28–31] and was used to realize an optical analog of event horizon [28].

The review is organized as follows. Section 2 presents a simple model that can be used to study propagation of optical pulses in a spatiotemporal dispersive medium. Section 3 uses this model to analyze the case of a single index boundary to discuss phenomena that are temporal analogs of the familiar spatial ones such as reflection, refraction, total internal reflection, and waveguiding. The use of solitons for creating moving index boundaries is considered in section 4, where we show that a pair of solitons can form the temporal analog of a waveguide or a Fabry–Perot resonator. Sections 5 is devoted to spatiotemporal Bragg gratings, forming when a train of solitons creates periodic high-index regions moving at the speed of pump pulses. The main results are summarized in section 6.

2. Modeling of dispersive media

A study of pulse propagation inside a spatiotemporal dispersive medium requires solutions of Maxwell's equations in a medium whose refractive index varies with both time and frequency, and may also vary spatially when the medium is in the form of an optical waveguide. In general, one must solve a four-dimensional wave equation that includes the effects of diffraction, dispersion, and a time-varying refractive index. To gain physical insight, it is important to simplify the problem by making suitable assumptions.

Considerable simplification occurs when the medium is in the form of a single-mode waveguide, such as an optical fiber. As the waveguide takes care of two transverse coordinates (x and y) for a beam propagating along the waveguide's length (the z axis), the problem is reduced to two dimensions involving the z and t variables. In this case, the electric field of an optical pulse can be written in the form

$$\mathbf{E}(\mathrm{r},t) = \mathrm{Re}\left[\hat{\mathbf{p}}F(x,y)A(z,t)\exp\left(\mathrm{i}\beta_0 z - \mathrm{i}\omega_0 t\right)\right], \qquad (1)$$

where $F(x,y)$ is the spatial profile of the single mode supported by the waveguide and $\hat{\mathbf{p}}$ is the unit vector representing the state of polarization, assumed to remain fixed. The function $A(z,t)$ is the slowly varying envelope of a pulse, launched with its spectrum centered at ω_0, and β_0 is the propagation constant at this frequency.

2.1. Propagation equation for pulses

The effects of chromatic dispersion are included by working in the frequency domain with the Fourier transform in the form

$$\tilde{A}(z,\omega) = \int_{-\infty}^{\infty} A(z,t)\,\mathrm{e}^{\mathrm{i}\omega t}\,\mathrm{d}t. \qquad (2)$$

Using Maxwell's wave equation, $\tilde{A}(z,\omega)$ is found to satisfy [27]

$$\frac{\partial\tilde{A}}{\partial z} = \mathrm{i}\left[\beta(\omega) - \beta_0\right]\tilde{A} + \mathrm{i}\left(\omega_0/c\right)n_1\tilde{A}, \qquad (3)$$

where $\beta(\omega) = (\omega/c)n_0(\omega)$, n_0 is the refractive index of the fiber's single mode before modulation is applied, and $n_1(t - z/v_m)$ is the index change produced by a wave traveling at the speed v_m. Frequency of this wave can vary over a wide range, depending on the physical process employed to produce index modulation. In the case of the Pockels effect, an electro-optic medium is employed with a microwave signal at frequencies

in the GHz range. In the case of the optical Kerr effect, a nonlinear medium is employed with pump pulses whose carrier frequency typically exceeds 200 THz.

It may appear strange that equation (3) is written in the frequency domain but contains a term that depends on time through $n_1(t-z/v_m)$. Its use can be justified by noting different time scales associated with the two terms in this equation. The first term involves the time scale of an optical cycle, while the second term varies on a much longer time scale. It is also quite small as n_1 is much smaller than n_0 in the frequency range of interest.

The frequency dependence of $n_0(\omega)$ depends on what role absorption plays. If ω is close to any resonance of the medium and absorption cannot be ignored, one must treat $n_0(\omega)$ as a complex quantity and use an appropriate model for it. However, silica glass used to make optical fibers does not exhibit much absorption in the 0.5–2 μm wavelength range [27]. In this situation, it is common to make use of the so-called dispersion parameters. When the pulse's spectrum is narrower compared to its central frequency ω_0, we can expand $\beta(\omega)$ in equation (3) using a Taylor series as

$$\beta(\omega) = \beta_0 + \beta_1(\omega-\omega_0) + \tfrac{1}{2}\beta_2(\omega-\omega_0)^2 + \ldots, \quad (4)$$

where $\beta_m = (d^m\beta/d\omega^m)_{\omega=\omega_0}$ with $m = 0, 1, 2, \ldots$. Limiting the expansion to $m = 2$, equation (3) becomes

$$\frac{\partial\tilde{A}}{\partial z} = \mathrm{i}\left[\beta_1(\omega-\omega_0) + \tfrac{1}{2}\beta_2(\omega-\omega_0)^2\right]\tilde{A} + \mathrm{i}(\omega_0/c)\,n_1\tilde{A}, \quad (5)$$

where β_1 and β_2 are the first- and second-order dispersion parameters. This approach allows one to include higher-order dispersion if necessary. Values of dispersion parameters can be calculated for silica fibers over a wide frequency range using the Sellmeier equation [27].

A time-domain equation is obtained by taking the inverse Fourier transform of equation (5), while treating the last term as being constant. This amounts to replacing $(\omega-\omega_0)$ with the differential operator $\mathrm{i}\frac{\partial}{\partial t}$. The final result is

$$\frac{\partial A}{\partial z} + \beta_1\frac{\partial A}{\partial t} + \frac{\mathrm{i}}{2}\beta_2\frac{\partial^2 A}{\partial t^2} = \mathrm{i}k_0 n_1(t-z/v_m)A, \quad (6)$$

where $k_0 = \omega_0/c = 2\pi/\lambda_0$ and λ_0 is the pulse's input wavelength. The last term includes the effects of spatiotemporal index modulation through $n_1(t-z/v_m)$. It proves useful to work in a frame in which modulation is stationary. For this purpose, we introduce a new time variable as $T = t - z/v_m$. In this moving frame, equation (6) becomes

$$\frac{\partial A}{\partial z} + \Delta\beta_1\frac{\partial A}{\partial T} + \frac{\mathrm{i}\beta_2}{2}\frac{\partial^2 A}{\partial T^2} = \mathrm{i}k_0 n_1(T)A, \quad (7)$$

where $\Delta\beta_1 = \beta_1 - 1/v_m$. As $\beta_1 = 1/v_g$, where v_g is group velocity of the pulse, the parameter $\Delta\beta_1$ is related to speed of the pulse relative to that of modulation.

Equation (7) is useful for studying a wide variety of spatiotemporal effects occurring inside a dispersive medium. This equation is linear because probe pulses are assumed to be relatively weak. For intense pulses, a nonlinear term of the form $i\gamma|A|^2A$ should be added to this equation [27].

Even without the nonlinear term, equation (7) resembles the nonlinear Schödinger (NLS) equation because of time-dependence of the last term. For this reason, it can be solved numerically with the same techniques used for solving the NLS equation. One such technique, known as the split-step Fourier method, alternates between the time and frequency domains for including the modulation and dispersive effects, respectively [27]. Another technique converts equation (7) to the frequency domain and employs the Runge–Kutta algorithm. We refer to [27] for further details.

2.2. Energy and momentum conservation

Conservation laws plays an important role in all branches of physics, including optics. In quantum mechanics, one relates energy to the number of photons contained within a pulse, which is a conserved quantity in most situations. The conservation of energy and momentum is also related to the translation symmetries in time and space, respectively. In a medium of constant refractive index, both of these symmetries exist. As a result, energy and momentum of each photon is conserved.

At a spatial interface with different refractive indices on its two sides, space translation symmetry is broken. As a result, energy of photons is conserved, but their momenta are not. This is why reflected and refracted waves can propagate in different directions when an optical wave crosses such an interface. Recall that a photon's momentum depends on its direction of propagation. At a temporal boundary across which refractive indices are different, it is the time translation symmetry that is broken. Thus, we expect the momentum to be conserved but energy of photons can change. As a photon's energy $\hbar\omega$ depends on the wave's frequency, it is the frequency of an incoming wave that changes during temporal reflection and refraction [6].

In the case of spatiotemporal index modulation, both translation symmetries are broken, and neither energy nor momentum is expected to be conserved. However, in the moving frame in which index modulation becomes stationary, the refractive index does not depend on the spatial coordinate z. As the space translation symmetry is preserved in this frame, momentum of all photons is conserved. Noting that the momentum of a photon of energy $\hbar\omega$ is related to the propagation constant as $\hbar\beta(\omega)$ at any frequency, $\beta(\omega)$ must remain conserved at all frequencies. As we will see later, this requirement can be used to study how the wavelength of a probe pulse changes as it propagates through a time-varying medium [8].

3. Moving index boundaries

The simplest situation of spatiotemporal index modulation corresponds to a moving boundary with different refractive indices on its two sides. In a frame moving at the boundary's speed, the boundary appears stationary, and we have the case of purely temporal modulation such that $n_1(T)$ in equation (7)

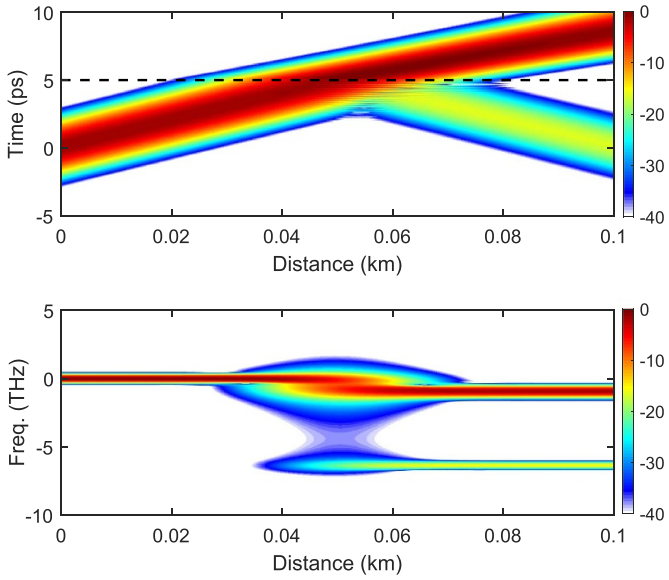

Figure 2. Temporal reflection and refraction of a Gaussian pulse at a temporal boundary (dashed line) inside a 100 m long fiber. Bottom parts shows frequency changes along the fiber's length. Reprinted (figure) with permission from [8], Copyright (2015) by the American Physical Society.

takes the form

$$n_1(T) = \delta n H(T - T_b), \tag{8}$$

where $H(x)$ is the Heaviside step function (1 for $x \geqslant 0$ and 0 otherwise) and δn is the magnitude of index change at the boundary located at $T = T_b$. Using this form in equation (7), we obtain [8]

$$\frac{\partial A}{\partial z} + \Delta\beta_1 \frac{\partial A}{\partial T} + \frac{i\beta_2}{2}\frac{\partial^2 A}{\partial T^2} = i\beta_b H(T - T_b)A, \tag{9}$$

where $\beta_b = k_0 \delta n$. This equation can be solved numerically to study how a probe pulse splits into its reflected and transmitted parts at the temporal boundary that move at different speeds because of a shift in their frequencies.

3.1. Temporal reflection and refraction

As an example of temporal reflection and refraction in a dispersive medium, figure 2 shows the results obtained by solving equation (9) numerically using $\Delta\beta_1 = 0.1$ ps m^{-1}, $\beta_2 = 5$ ps^2 km^{-1}, and $\beta_b = 0.5$ m^{-1}, values appropriate for a silica fiber [8]. The probe pulse at the input end of the 100 m long is assumed to have a Gaussian shape such that $A(0,T) = A_0 \exp(-T^2/2T_0^2)$ with $T_0 = 1$ ps. The index change required at the boundary, located at $T_b = 5$ ps (dashed line), is $<10^{-7}$ for the parameter values used.

Temporal evolution in figure 2 (top part) shows how a probe pulse splits into its reflected and refracted parts, when it arrives at the boundary where refractive index increases slightly. As seen in the bottom panel, both parts experience frequency shifts such that their spectra are red-shifted (a negative frequency shift). The magnitude of frequency shift is <1 THz for the transmitted part but exceeds 6 THz for the reflected pulse. Physically, the probe pulse splits into two parts that travel at different speeds because of spectral shifts. The reflected part does not cross the boundary because of its much larger frequency shift. Blue shifts occur when β_2 is negative at the wavelength of probe pulses.

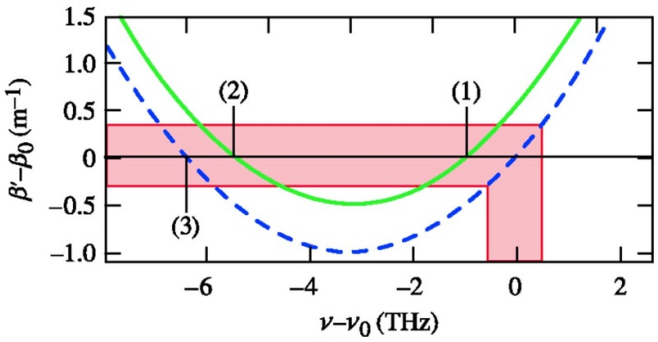

Figure 3. Parabolic dispersion curves before (dashed line) and after (solid line) the boundary. The red region corresponds to spectral bandwidth of pulses.

Spectral shifts can be calculated by invoking the conservation of momentum in the moving frame in which boundary is stationary. As discussed in section 2.2, this requires $\beta(\omega)$ to remain unchanged for the reflected and transmitted parts from its initial value at every frequency within the probe's spectrum. Figure 3 shows the matching procedure graphically using the parabolic dispersion curves before (dashed) and after the boundary. Consider a frequency shifted from ω_0 by $\Delta\omega = \omega - \omega_0$. Writing equation (4) in the moving frame, we obtain the following relation for $\Delta\beta = \beta - \beta_0$:

$$\Delta\beta(\Delta\omega) = \Delta\beta_1 \Delta\omega + \tfrac{1}{2}\beta_2 (\Delta\omega)^2 + \beta_b. \tag{10}$$

The last term is present only for the transmitted part that crosses the boundary.

Let $\Delta\omega_r$ and $\Delta\omega_t$ be the frequency shifts when probe's frequency is $\omega_0 + \Delta\omega$. Using $\Delta\beta(\Delta\omega_r) = \Delta\beta(\Delta\omega)$, frequency of the reflected part is found to be

$$\Delta\omega_r = -\Delta\omega - (2\Delta\beta_1/\beta_2). \tag{11}$$

Similarly, frequency of the transmitted part is found using $\Delta\beta(\Delta\omega_t) = \Delta\beta(\Delta\omega)$. This requirement results in a quadratic equation, whose physically relevant solution is given by

$$\Delta\omega_t = -\frac{\Delta\beta_1}{\beta_2} + \frac{1}{\beta_2}\left[(\Delta\beta_1 + \beta_2\Delta\omega)^2 - 2\beta_b\beta_2\right]^{1/2}. \tag{12}$$

Several features of the frequency shifts in equations (11) and (12) are noteworthy. While $\Delta\omega_r$ depends only on the fiber's dispersion parameters and speed of the boundary, $\Delta\omega_t$ also depends on the index change occurring at the boundary. It is remarkable that both frequency shifts do not depend on the probe-pulse parameters. Note also that shifts can be positive or negative (blue or red shifts), depending on the signs of the fiber's parameters involved. Both $\Delta\beta_1$ and β_2 can be positive or negative depending on the probe's wavelength and its speed

relative to the boundary. The frequency shifts seen in figure 2 agree well with the preceding two analytic expressions.

It is possible to obtain analytic expressions for the reflection and transmission coefficients at a given frequency. By matching the boundary conditions on the two sides of the temporal boundary, these are found to depend on the frequency shifts given in equations (11) and (12) as [25]:

$$R(\Delta\omega) = \frac{\Delta\omega_t - \Delta\omega}{\Delta\omega_r - \Delta\omega_t}, \quad T(\Delta\omega) = \frac{\Delta\omega_r - \Delta\omega}{\Delta\omega_r - \Delta\omega_t}, \tag{13}$$

with an additional phase $(\Delta\omega_t - \Delta\omega)T_b$ that depends on the boundary's location T_b.

The expressions in equation (13) can be used to find the amplitudes of reflected and transmitted pulses by working in the frequency domain and using the Fourier transform as indicated in equation (2). For the input pulse, we have

$$\tilde{A}_i(\Delta\omega) = \int_{-\infty}^{\infty} A_i(t)\, \mathrm{e}^{\mathrm{i}\Delta\omega t}\, \mathrm{d}t. \tag{14}$$

Each spectral component $\tilde{A}_i(\Delta\omega)$ undergoes reflection and refraction at the temporal boundary. Since the problem is linear, the amplitudes of reflected and transmitted pulses can be written as

$$A_r(z,T) = \frac{1}{2\pi}\int_{-\infty}^{\infty} \tilde{A}(\Delta\omega)\, R(\Delta\omega) \times \exp\left[\mathrm{i}\beta(\Delta\omega_r)z - \mathrm{i}\Delta\omega_r t\right] \mathrm{d}\Delta\omega, \tag{15}$$

$$A_t(z,T) = \frac{1}{2\pi}\int_{-\infty}^{\infty} \tilde{A}(\Delta\omega)\, T(\Delta\omega) \times \exp\left[\mathrm{i}\beta(\Delta\omega_t)z - \mathrm{i}\Delta\omega_t t\right] \mathrm{d}\Delta\omega. \tag{16}$$

3.2. Total internal reflection(TIR)

The expression in equation (12) points to the possibility of TIR of the probe pulse at a moving boundary. To see this clearly, focus on the central frequency of the pulse and set $\Delta\omega = 0$ in equation (12) to obtain

$$\Delta\omega_t = -\frac{\Delta\beta_1}{\beta_2} + \frac{1}{\beta_2}\left[(\Delta\beta_1)^2 - 2\beta_b\beta_2\right]^{1/2}. \tag{17}$$

Notice that $\Delta\omega_t$ becomes a complex quantity when the index change δn across the boundary is large enough to satisfy the relation $2\beta_b\beta_2 > (\Delta\beta_1)^2$. As transmission of power across the boundary cannot occur in this case, only a reflected pulse is produced at the shifted wavelength. This temporal analog of TIR differs from the conventional TIR in one respect. Whereas spatial TIR requires light to travel from a high-index region to a low-index one, temporal TIR has no such restriction. This is because the dispersion parameter β_2 in equation (17) can take both positive and negative values, depending on the wavelength of incident light. When β_b is negative, β_2 should also be negative for the TIR to occur.

As an example of TIR, numerical results shown in figure 4 were obtained under the same conditions used for figure 2, except that the value of β_b was larger by a factor of three [8].

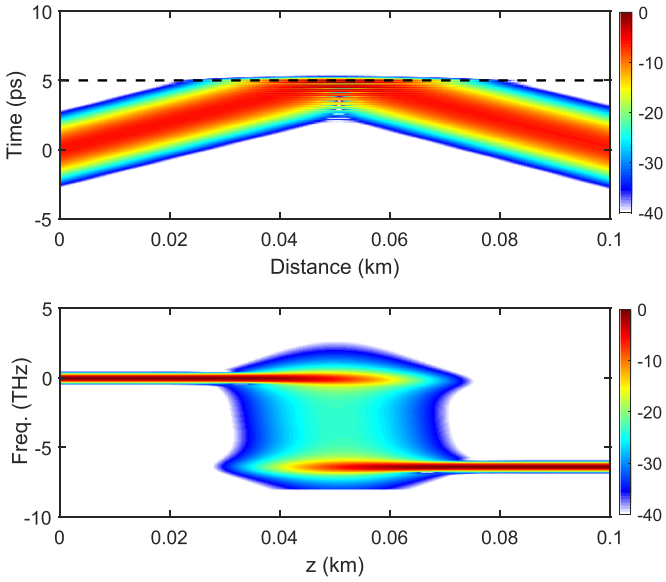

Figure 4. Same as figure 2 except for a larger index change at the boundary ($\beta_b = 1.5\ \mathrm{m}^{-1}$). The absence of refracted part indicates total internal reflection in the time domain. Reprinted (figure) with permission from [8], Copyright (2015) by the American Physical Society.

As seen there, the probe pulse undergoes TIR at the spatiotemporal boundary (dashed black line), and its spectrum shifts by more than 6 THz. The index change required for this phenomenon to occur is only 2.2×10^{-7} at probe wavelengths near 1 μm. Simulations show that, similar to the spatial case, an evanescent wave exists on the other side of the temporal boundary.

In the case of a spatial interface, TIR is accompanied with the Goos–Hänchen effect [32], which corresponds to a shift of the reflected beam's center relative to its position expected for normal reflection. One would expect such a shift to occur in the temporal case as well. Recent work has shown that this is indeed the case [33]. The following analytic expression provides temporal shift of the TIR pulse:

$$\Delta\tau_{\mathrm{GH}} = \frac{2\,\mathrm{sgn}(\Delta\beta_1)\,\beta_2}{\sqrt{2\beta_b\beta_2 - (\Delta\beta_1)^2}}. \tag{18}$$

Numerical simulations based on equation (7) show clearly such a temporal shift. As an example, figure 5 shows the evolution of a a 6 ps wide Gaussian pulse undergoing TIR inside an optical fiber using $\beta_2 = 0.05\ \mathrm{ps}^2\ \mathrm{m}^{-1}$, $\Delta\beta_1 = 0.25\ \mathrm{ps}\ \mathrm{m}^{-1}$, and $\beta_b = 1\ \mathrm{m}^{-1}$. The bottom part shows the temporal shift induced by the Goos–Hänchen effect. The shift seen here agrees well with the predicted value, $\Delta\tau_{\mathrm{GH}} = 0.516$ ps, based on equation (18).

3.3. Temporal waveguides

Similar to the spatial case, time-domain TIR can be used to realize the temporal analog of an optical waveguide, which confines a beam spatially to its high-index core, sandwiched

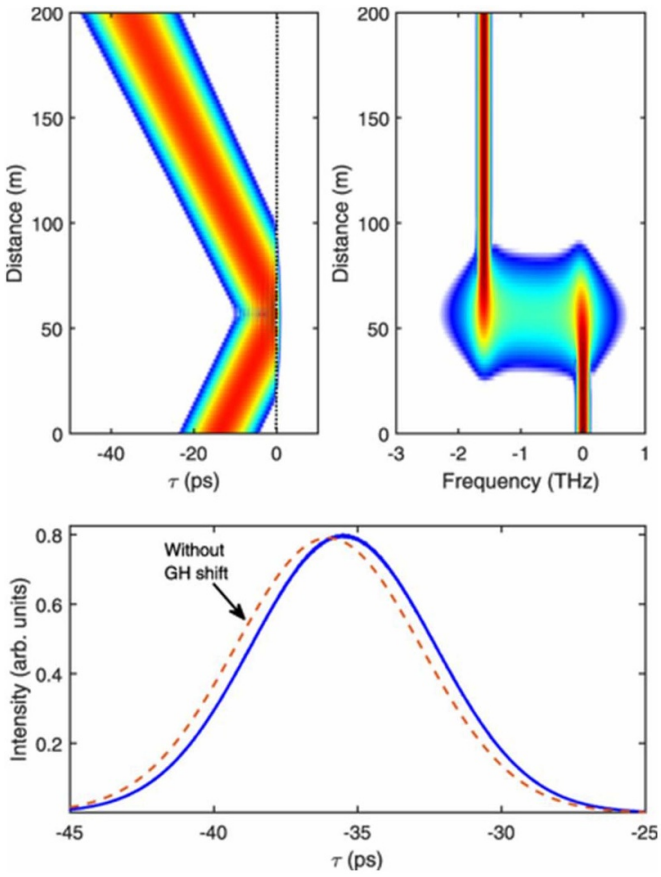

Figure 5. TIR of a 6 ps wide Gaussian from a moving index boundary inside an optical fiber; (top) evolution in the time and frequency domains; (bottom) intensity profile of reflected pulse with (solid) and without (dashed) the Goos–Hänchen effect. Reprinted (figure) with permission from [33], Copyright (2022) by the American Physical Society.

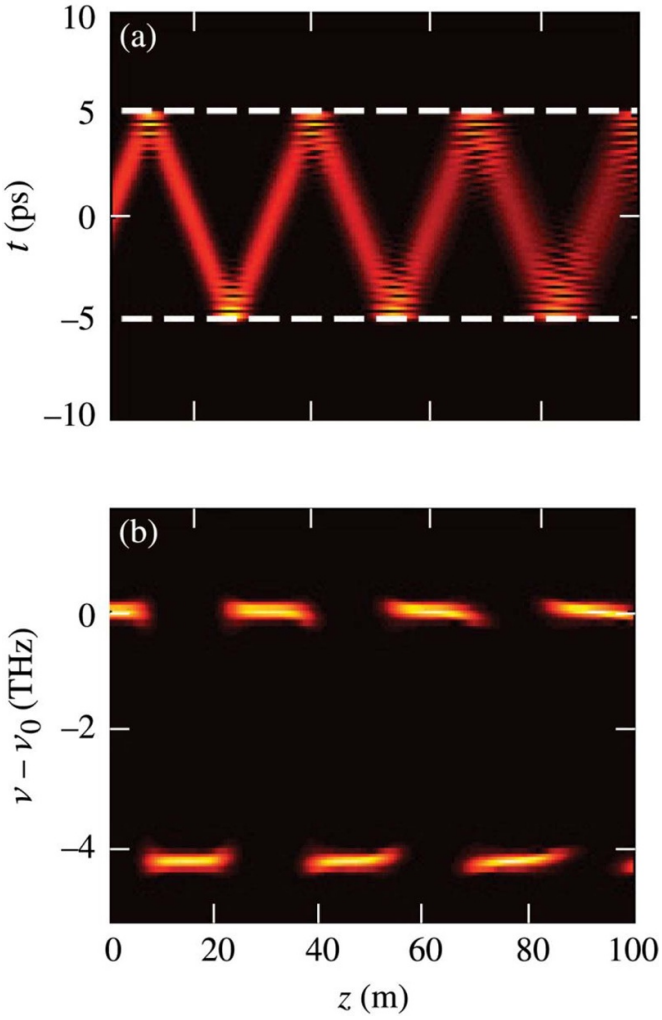

Figure 6. Evolution of the (a) shape and (b) spectrum of a Gaussian pulse inside a 10 ps wide temporal waveguide. Dashed lines indicate the time window that forms the waveguide's core. Adapted with permission from [23] © The optical Society.

between two cladding layers. In the temporal case, a pulse is confined to a time window, where refractive index differs from the regions outside of that widow [23]. The confinement process can be understood as follows. An optical pulse, located in the middle of the time window, travels toward one of its boundaries and is reflected from it. The spectrum of reflected pulse is modified such that it slows down and moves away from the first boundary. When the pulse arrives at the second boundary, it again experiences TIR such that its center frequency reverts back to the original value. This process repeats itself, trapping the pulse inside the time window.

Figure 6 shows the stimulated evolution of a 2.5 ps Gaussian pulse along a 100 m long optical fiber using $\Delta\beta_1 = 0.667$ ps m^{-1} and $\beta_2 = 0.05$ ps^2 m^{-1}. The refractive index is different inside the 10 ps time window because $\beta_b = 5.6$ m^{-1} for $|T| < 5$ ps but 0 outside of this time window. as seen in part (a), the pulse bounces back and forth between the two temporal boundaries. Reflection at the top boundary produces a frequency shift of -4.25 THz, which changes the pulse's speed such that it moves toward the lower boundary. When the pulse is reflected from this boundary, its center frequency is shifted back to the original value, and this process repeats with further propagation. Temporal fringes seen near the two boundaries result from interference between two frequency-shifted pulses overlapping in this region.

The evolution seen in figure 6 is analogous to that observed in multimode waveguides, designed with a core much wider than the beam's width. This suggests that one should analyze whether temporal waveguides support modes that are analog of the spatial modes of planar waveguides. For this purpose, we need solutions of equation (7) that do not change with propagation except for a phase shift:

$$A(z,t) = M(t)\exp\left[\mathrm{i}\left(Kz - \Omega t\right)\right], \tag{19}$$

where $M(t)$ is the temporal shape of the mode, K is the rate at which this mode accumulates phase, and Ω is a frequency shift, occurring because of the first-derivative term in equation (25).

Substituting equation (19) into equation (9) and equating the real and imaginary parts, we obtain

$$(\Delta\beta_1 + \beta_2\Omega)\frac{\mathrm{d}M}{\mathrm{d}t} = 0, \tag{20}$$

$$\frac{\mathrm{d}^2M}{\mathrm{d}t^2} + \frac{2}{\beta_2}\left(K - \Omega\Delta\beta_1 - \frac{\beta_2\Omega^2}{2} - \beta_b\right)M = 0. \tag{21}$$

From equation (20), the frequency shift for all modes is found to be $\Omega = -\Delta\beta_1/\beta_2$. Using this value of Ω in equation (21), the modes are found by solving

$$\frac{\mathrm{d}^2M}{\mathrm{d}t^2} + \frac{2}{\beta_2}\left(K + \frac{(\Delta\beta_1)^2}{2\beta_2} - \beta_b\right)M = 0. \tag{22}$$

This is an eigenvalue equation whose solutions provide temporal shapes of modes for specific values of the eigenvalue K.

At this point, one can follow the same procedure used for spatial waveguides to find the temporal profiles of different modes [23]. Similar to the spatial case, we can introduce a dimensionless parameter as

$$V = \sqrt{\left(2\beta_b T_b^2\right)/\beta_2}. \tag{23}$$

This parameter determines the number of modes supported by a temporal waveguide of width $2T_b$. In analogy with the spatial case, the waveguide supports m modes when $V < (m+1)\pi/2$. In particular, a temporal waveguide supports only a single mode ($m = 0$) if it is designed such that $V < \pi/2$. The waveguide in figure 6 supports 48 modes because the value of V is close to 75 for it. If we change the value of β_b by a factor of 2000, the same 10 ps wide waveguide would support a single mode. When the width of input pulse is matched to the width of this mode (about 5 ps), it excites a single mode and remains confined to the temporal waveguide.

Figure 7 shows the evolution of a Gaussian pulse with $I(t) = I_0\exp(-T^2/T_0^2)$ using $T_0 = 2.5$, 5, and 10 ps. The 2.5 ps pulse in part (a) quickly broadens because of dispersion. The pulse sheds considerable energy outside the core region as it reshapes itself into the fundamental mode of the waveguide. In contrast, the 10 ps pulse in part (c) is wider than the waveguide and only a fraction its energy is guided. The 5 ps pulse in part (b) is just wide enough that most of its energy lies inside the temporal waveguide. Such a width adjustment is analogous to mode-matching required for spatial waveguides.

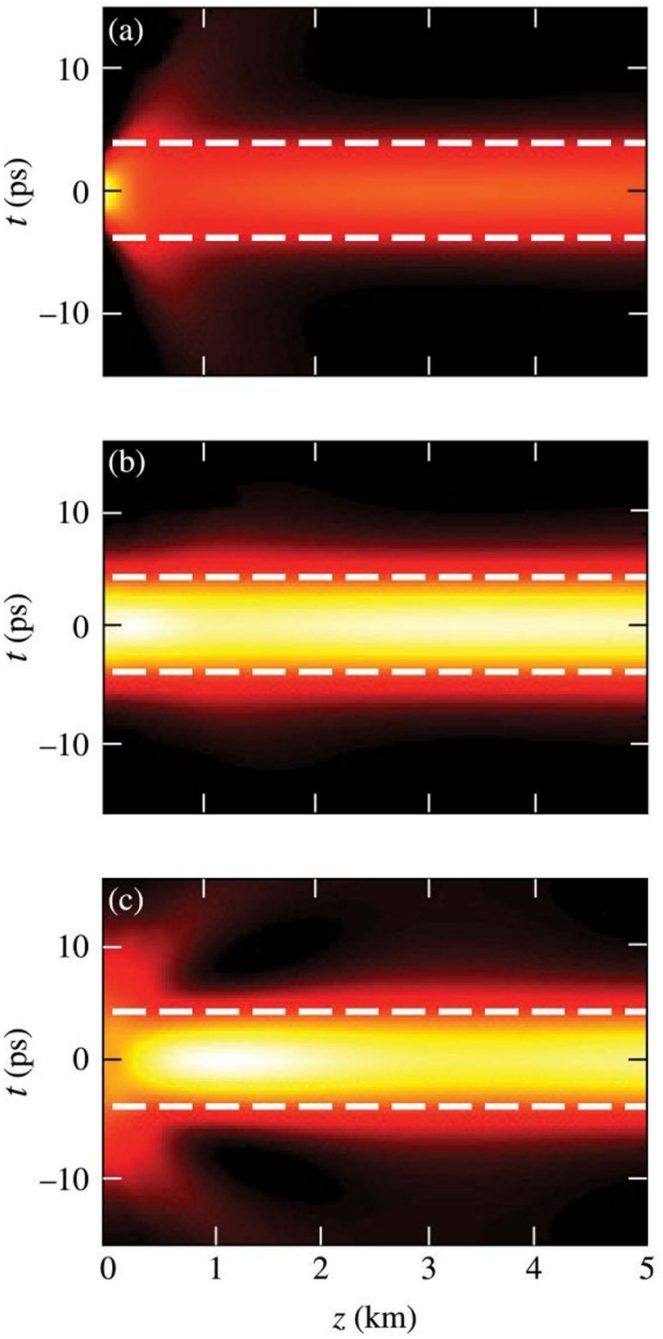

Figure 7. Mode-matching in temporal waveguides. The initial width T_0 of the Gaussian pulse is (a) 2.5 ps, (b) 5 ps, and (c) 10 ps. Adapted with permission from [23] © The optical Society.

4. Pump-probe configuration

This section shows how a spatiotemporal boundary can be formed inside a dispersive medium such that it has different refractive indices on its opposite sides. A mechanism is needed that uses a traveling wave to change the refractive index n of a suitable material. As n must change rapidly, thermal and acoustic effects are too slow to be useful. One possibility is to make use of the Pockels effect inside a waveguide, made with an electro-optic material such as $LINbO_3$ [34]. The electric field of a microwave can then produce an index boundary moving at the speed of the microwave signal. This technique provides index changes at a time scale ~100 ps, which may not be fast enough for practical applications. It is also limited by typical lengths of $LINbO_3$ waveguides (10 cm or less).

The use of optical Kerr effect solves both of these problems. This effect manifests as a nearly instantaneous change in the refractive index of a nonlinear material such that $n(t) = n_0 + n_2 I(t)$, where n_2 is the material's Kerr coefficient and $I(t)$ is the intensity of optical pulses launched into that medium [34]. If silica fibers are employed for this purpose, their low losses permit fiber lengths as long as a few kilometers. A

pump-probe configuration is employed in practice such that pump and probe pulses of different wavelengths are launched into an optical fiber with a controllable separation between the two. Pump pulses create a moving high-index region, and probe pulses interact with it through the nonlinear phenomenon of cross-phase modulation [27].

4.1. Solitons as moving boundaries

The use of pump pulses inside optical fibers still suffers from one problem. In general, pump pulses would become distorted because of the dispersive and nonlinear effects, resulting in a high-index boundary that does not maintain itself over the fiber's length. This problem can be solved by making use of optical solitons. It is well known [27] that solitons can form when pump pulses are launched at a wavelength longer than the zero-dispersion wavelength of the fiber so that the group-velocity dispersion (GVD) is anomalous, and the parameter β_2 is negative. When the width and peak power (T_s and P_s) of pump pulses are chosen such that $N^2 = \gamma P_s T_s^2/|\beta_{2p}| = 1$, where N is the soliton's order, the shape of pump pulses does not change as they travel down an optical fiber. The nonlinear parameter γ is related to the Kerr coefficient n_2 as $\gamma = k_0 n_2/A_{\rm eff}$, where $A_{\rm eff}$ is the effective area of the single mode supported by the fiber.

Pump pulses evolve inside an optical fiber according to the NLS equation [27]:

$$\frac{\partial A_p}{\partial z} + \frac{i\beta_{2p}}{2}\frac{\partial^2 A_p}{\partial T^2} = i\gamma|A_p|^2 A_p. \tag{24}$$

where A_p is the slowly varying amplitude of pump pulses. This equation can be obtained from equation (7) by setting $\Delta\beta_1 = 0$ and replacing n_1 with the nonlinear index change $n_2 I$, where $I = |A_p|^2/A_{\rm eff}$. When it is solved with the initial condition, $A_p(0) = \sqrt{P_s}\,\mathrm{sech}(T/T_s)$, and P_s is chosen such that $N = 1$, each pump pulse forms a fundamental soliton, and its shape, width, and peak power do not change with distance z. In this situation, the medium's refractive index increases over the soliton's duration and is the largest at the peak of the soliton. This increase in n creates a spatiotemporal boundary, moving at the speed of pump pulses. A probe pulse sees this increase such that $\beta_b = 2\gamma|A_p|^2$, where the factor of 2 results from cross-phase modulation [27]. In practice, maximum index change δn is limited to values below 10^{-6}. As we have seen in section 3, such values are large enough to observe temporal reflection and waveguiding.

The probe's evolution is governed by equation (7), but $k_0 n_1$ should be replaced with $\beta_b = 2\gamma|A_p|^2$. It is also useful to introduce normalized variables as $\tau = T/T_0$ and $\xi = z/L_D$, where $L_D = T_0^2/|\beta_2|$ is the dispersion length. The resulting equation becomes

$$\frac{\partial A}{\partial \xi} + d\frac{\partial A}{\partial \tau} + \frac{i}{2}\frac{\partial^2 A}{\partial \tau^2} = iC_x \mathrm{sech}^2(\tau/\tau_s)A, \tag{25}$$

where $d = \Delta\beta_1 L_D$, $\tau_s = T_s/T_0$, and $C_x = 2\gamma P_s L_D$ are three dimensionless parameters. This equation can be solved numerically to study the evolution of a probe pulse and its interaction with a pump soliton inside a silica fiber. In the moving fame, soliton's peak remains fixed at $\tau = 0$.

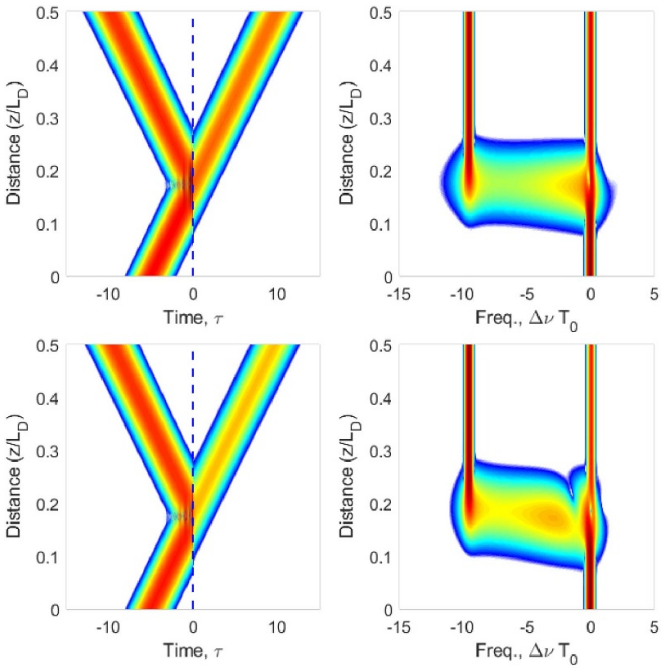

Figure 8. Reflection and refraction of a Gaussian pulse by a soliton that is 10 times (top) or 5 times (bottom) shorter than the pulse. Temporal and spectral evolutions are shown in both cases. The vertical dashed line marks soliton's peak.

Figure 8 shows the temporal reflection and refraction of a Gaussian pulse when it collides with a pump soliton, whose width is 10 times shorter than its own width, using $d = 30$ and $C_x = 500$. For comparison, bottom part shows changes occurring when soliton is only 5 times shorter than the probe pulse ($\tau_s = 0.2$). When a soliton is used to form a spatiotemporal boundary, its width plays an important role because it dictates the sharpness of this boundary. A shorter soliton produces a sharper boundary. One may naively think that reflection will be reduced for a wider soliton. However, as seen in figure 8, the opposite happens. Nearly total reflection occurs when soliton is only half as wide as the probe pulse.

The impact of a boundary's sharpness on temporal reflection was studied in 2021 using a transfer-matrix approach with a staircase model for shallow boundaries [26]. The results show that the frequency range over which reflection can occur is reduced as rise time increases. However, TIR persists even for shallow boundaries with long rise times. This feature suggests that solitons cane be used as time-domain mirrors even when pump pulses have relatively long rise and fall times.

4.2. Fabry–Perot resonators (FPR)

A conventional FPR consists of two partially reflecting mirrors that enclose a dielectric medium of refractive index n. The transmission spectrum of such a device exhibits a periodic array of resonances occurring at frequencies $\nu_m = mc/(2nL_r)$, where m is an integer and L_r is the resonator's length (gap between two mirrors). Such devices are routinely used for

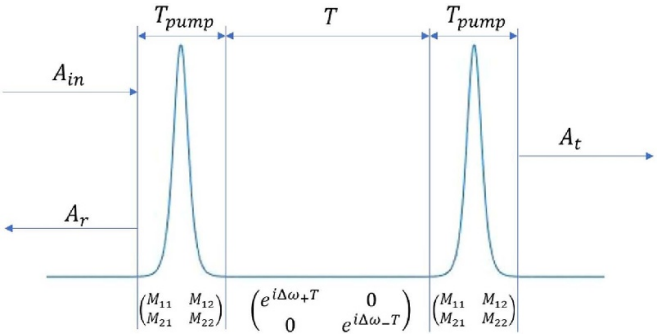

Figure 9. Schematic of a time-domain FPR. Two identical solitons act as partially reflecting mirrors. The bottom part shows transfer matrices of three sections.

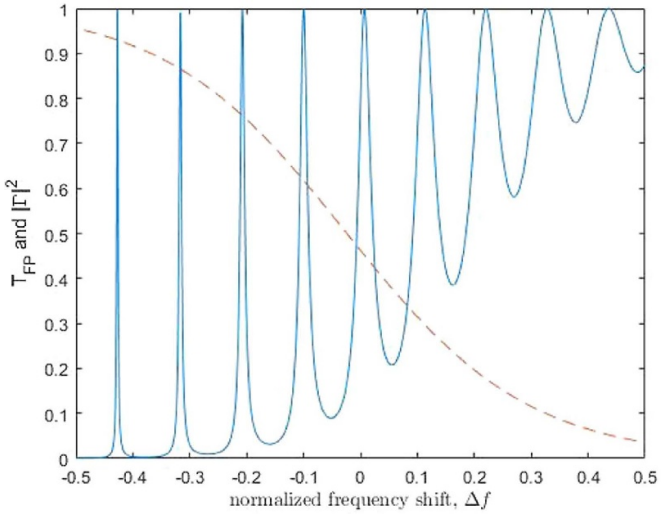

Figure 10. Frequency dependence of T_{FP} (solid curve) and $|\Gamma|^2$ (dashed curve) for the FPR formed using two solitons acting as temporal mirrors. Adapted with permission from [35] © The optical Society.

spectral analysis because they provide a frequency comb with a controllable spacing among its comb lines.

As we have seen, solitons inside an optical fiber act effectively as mirrors in the time domain. One can construct the temporal analog of a FPR by using two such solitons, separated by a fixed interval T_f [35]. Figure 9 shows such a time-domain FPR schematically.

When a probe pulse is incident at such a FPR, it can be transmitted or reflected, depending on whether its spectrum falls within or outside of a resonance peak. The transmission spectrum of the FPR is calculated by considering each frequency component of the probe separately. A transfer matrix approach was used in one study [35] by dividing the FPR into three sections, as shown in figure 9. If M is the transfer matrix of each soliton section, the transfer matrix of the entire FPR becomes:

$$F = \begin{pmatrix} M_{11} & M_{12} \\ M_{21} & M_{22} \end{pmatrix} \begin{pmatrix} \mathrm{e}^{\mathrm{i}\Delta\omega_+ T_f} & 0 \\ 0 & \mathrm{e}^{-\mathrm{i}\Delta\omega_- T_f} \end{pmatrix} \begin{pmatrix} M_{11} & M_{12} \\ M_{21} & M_{22} \end{pmatrix}, \tag{26}$$

where $\Delta\omega_\pm$ are the frequency shifts for the forward and backward propagating waves inside the FPR. They are obtained from equation (12) after replacing the $+$ sign of the last term with a $\pm$ sign.

The transmissivity of the FPR is found from the preceding relation to be [35]

$$T_{\mathrm{FP}} = \left(1 + \frac{4|\Gamma|^2}{(1-|\Gamma|^2)^2} \sin^2 \frac{\phi}{2}\right)^{-1}, \tag{27}$$

with $\Gamma = M_{21}/M_{11}$ is the reflection coefficient of each soliton. The phase shift depends on the width and separation of two solitons as

$$\phi = (\Delta\omega_+ - \Delta\omega_-)\, T_f + 2\Delta\beta_1 T_s/\beta_2 + 2\phi_0, \tag{28}$$

where ϕ_0 is the phase of the matrix element M_{11}. Equation (27) resembles the corresponding expression found for standard FPRs. Its form is an example of the underlying space-time duality in optics.

As an example, we consider a FPR made with two 80 fs solitons ($T_s = 50$ fs), separated by 1.4 ps, and use $\beta_b = 1.2$ m^{-1}, $\beta_2 = 5$ ps^2 km^{-1}, $\Delta\beta_1 = 0.1$ ps m^{-1} for the parameters. We calculate Γ first and use its value in equation (27) to find T_{FP} of the FPR as a function of normalized frequency shift $\Delta f = (\beta_2/\Delta\beta_1)\Delta\omega_+$. The results are shown in figure 10, where both T_{FP} and $|\Gamma|^2$ are plotted. Similar to the spatial case, T_{FP} shows multiple resonances width 100% transmission at each peak. However, successive peaks do not maintain the same width and contrast, a situation quite different from the spatial case. This feature can be understood by noting that the reflectivity $|\Gamma|^2$ of each soliton decreases as Δf increases, whereas it remains nearly constant for a conventional mirror.

To see how the response of a temporal FPR depends on the spectrum of a probe pulse, We simulate numerically the transmission of a relatively wide Gaussian pulse ($T_0 = 20$ ps) through the same FPR used for figure 10. Figure 11 show the temporal evolution of the probe when its spectrum (a) fits within a transmission peak or (b) falls in between two peaks. Part (d) shows the location of the pulse's spectrum in the two cases within the transmission spectrum of the FPR. Time-varying index changes induced by two solitons are shown in part (c). As expected, the probe pulse is almost fully transmitted when its spectrum falls within a transmission peak. In contrast, it is mostly reflected when its spectrum falls in the middle of two transmission peaks.

4.3. Soliton-based waveguides

The double-soliton configuration, shown in figure 9, can also be used for making a temporal waveguide that confines probe pulses to the region between two solitons. Such a waveguide is realized by ensuring that both solitons reflect the probe pulse through the TIR process. When the pump and probe probe pulses are launched into an optical fiber such that the probe pulse is located between the two pump pulses, it is trapped

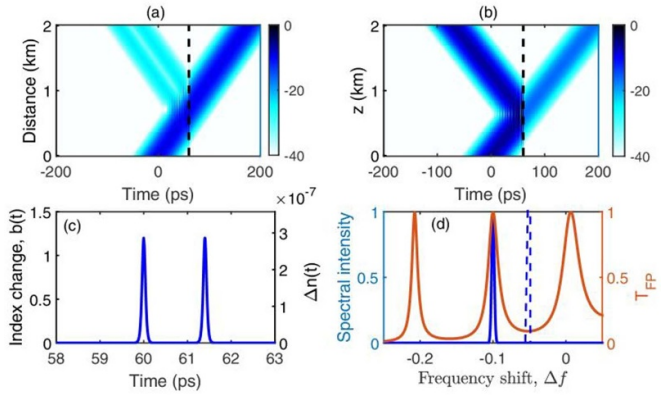

Figure 11. Temporal evolution of a 20 ps Gaussian pulse when its spectrum is (a) centered at a transmission peak and (b) falls outside of it. (c) Index change induced by solitons. (d) Location of pulse's spectra within the transmission spectrum. Adapted with permission from [35] © The optical Society.

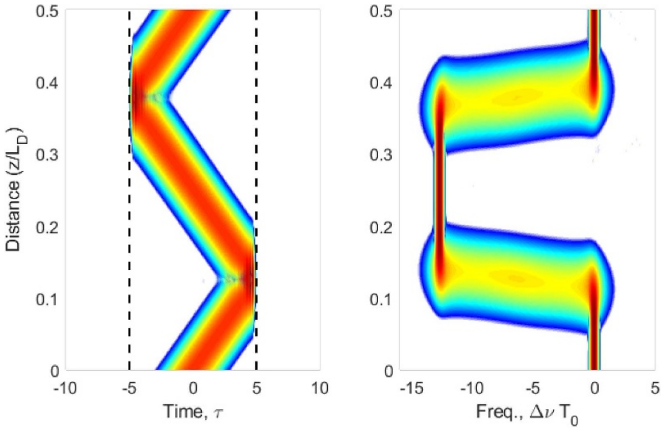

Figure 12. Evolution of the (a) shape and (b) spectrum of a Gaussian pulse inside a temporal waveguide formed by two solitons acting as totally reflecting mirrors. Dashed vertical lines mark the core region of this waveguide.

within the core of the temporal waveguide formed by the two solitons.

Figure 12 shows how such a waveguide functions by solving The NLS equation (25) numerically. It depicts the temporal and spectral evolutions along the fiber's length when the Gaussian-shape probe pulse of width T_0 is located initially in the middle of two pump solitons separated by $10T_0$. In normalized units, equation (25) was solved with the initial amplitude $A(0,\tau) = \exp(-\tau^2/2)$ using parameters values $d = 40$, $\tau_s = 0.1$ and $C_x = 1000$. The two solitons located at $\tau = \pm 5$ were 10 times shorter than the probe. These results apply for probe pulses of any width. For probe pulses launched at a wavelength near 1.1 μm with $T_0 = 1$ ps, the required fiber length is under 100 m. The wavelength of 100 fs pump pulses should be near 1.5 μm to ensure anomalous GVD needed for the two solitons.

Figure 12 should be compared with figure 6 drawn for a generic temporal waveguide. The time-domain behavior is similar in the two cases, but differences are apparent in the spectral domain when solitons are used for making a temporal waveguide,. More specifically, the probe pulse bounces back and forth between the two temporal boundaries formed by the two pump pulses propagating as solitons. The TIR at the $\tau = 5$ boundary is accompanied with a large frequency shift of about $-13/T_0$ THz, which changes the probe's speed such that it begins to moves toward the other soliton located at $\tau = -5$. Notice the distinctive pattern of the probe's spectral shift. When this probe pulse is reflected from the second soliton, its center frequency is shifted back to the original value. As discussed in section 3.3, the core of this temporal waveguide is much wider than the probe's width, resulting in the excitation of multiple modes. A single-mode waveguide can be formed by reducing the probe's width such that it matches the width of the core's fundamental mode. However, mode-matching is difficult in the case of solitons because the core's edges are not sharp even for short solitons.

4.4. Experiments

Temporal reflection has certainly been seen in many experiments on supercontinuum generation [36], where a higher-order soliton breaks into many fundamental solitons, which generate dispersive waves that can play the role of a low-energy probe pulse [27]. Moreover, it often plays a positive role by extending the supercontinuum toward the blue side. More direct evidence of temporal reflection has occurred in the experiments interpreted as the creation of an optical analog of the 'event horizon' by a soliton [28–31]. In these experiments, a high-index region, created inside an optical fiber by a soliton, reflects the probe with substantial frequency shifts.

Most clear evidence of temporal reflection occurred in a 2012 experiment [30], performed by using a 1.1 m long microstructured fiber, whose zero-dispersion wavelength was in the visible region near 710 nm. This allowed the use of 105 fs pulses at 810 nm for forming solitons in the anomalous-GVD region of the fiber. The wavelength of probe pulses was in the normal-GVD region at wavelengths near 620 nm so that pulses traveled at nearly the speed of pump pulses. When the wavelength of probe pulses was varied from 595 to 645 nm, either a blue shift or red shift occurred for the reflected pulse, depending on whether the probe was traveling faster or slower than the soliton. These features agree with the theory in section 4.1.

To the author's knowledge, no experiment has yet been carried out to verify the predictions of section 4.2 for time-domain FPRs. However, a clear evidence of the formation of a temporal waveguide by two solitons was seen in a 2015 experiment through a pump-probe type experiment [37]. Pump pulses used to form soliton pairs inside a 29 m long photonic crystal fiber (zero-dispersion wavelength near 980 nm) were 250 fs wide, and their wavelength was tunable from 1000–1500 nm. Probe pulses were considerably wider, and their 802 nm wavelength was in the normal-GVD region of the fiber. Spectral measurements showed clearly how the wavelength of each probe pulse shifted back and forth, as it was reflected from the two solitons forming the waveguide's core (see

figure 12). Hopefully, this review will stimulate further experimental work on the concepts covered in section 4 and the next section devoted to spatiotemporal Bragg gratings (STBG).

5. STBG

As we saw in section 4, a single soliton acts as a time-domain mirror, and two such mirrors can be used for making a FPR or a temporal waveguide. It is natural to ask what happens when several solitons act as partially reflecting mirrors. Each soliton increases the refractive index by a small amount (typically $<10^{-6}$) over its duration. If solitons are separated equally in time, the resulting periodic index changes produce a situation that is a time-domain analog of a Bragg grating. However, as solitons are moving at the speed of pump pulses, the Bragg grating is also moving at the same speed inside the optical fiber containing these solitons. Such STBG were recently found to exhibit several interesting novel features [38]. The temporal analog of a static Bragg grating has also been discussed but without including the dispersive effects of the medium [39].

A non-moving temporal Bragg grating is closely related to photonic time crystals that have attracted considerable attention in recent years [13, 16, 40]. In contrast to spatial crystals, which exhibit energy gaps in their band structure, photonic time crystals exhibit momentum gaps in their band structure. These gaps occur when frequencies of the eigenmodes become imaginary in specific ranges of the wave number **k**. We expect such gaps to occur for a STBG as well.

5.1. Physical model

The formation of a STBG through the Kerr nonlinearity requires that a train of pump pulses maintain its structure (the shape, width, and interpulse spacing) during its propagation inside an optical fiber. This is possible if each pump pulse propagates as a fundamental soliton, and solitons are kept far apart enough that their nonlinear interaction is negligible. In this situation, the nonlinear index change induced by the Kerr effect varies with time as [27]

$$\delta n\,(T) = \frac{n_2 P_s}{A_{\rm eff}} \sum_m \mathrm{sech}^2\left(\frac{T - mT_d}{T_s}\right), \tag{29}$$

where the sum is over all pulses within the soliton train and two neighboring solitons are separated in time by T_d. Clearly, the refractive index of the fiber's mode increases in a periodic fashion over the duration of each soliton, creating a moving Bragg grating.

The moving Brag grating affects the propagation of a probe pulse launched at a different wavelength into the same fiber. To study the evolution of this probe pulse, we use equation (7) and include the probe's interaction with pump pulses through XPM as [8]:

$$\frac{\partial A}{\partial z} + \Delta\beta_1 \frac{\partial A}{\partial T} + \frac{\mathrm{i}\beta_2}{2}\frac{\partial^2 A}{\partial T^2} = 2ik_0 \delta n\,(T) A, \tag{30}$$

where the factor of two on the right side results from index changes induced through the nonlinear phenomenon of XPM [27].

By choosing the reference frequency ω_0 suitably, one can eliminate the $\Delta\beta_1$ term in equation (30). We choose ω_0 as the frequency for which $\Delta\beta_1$ vanishes (probe' frequency differs from it by a fixed amount). It is also useful to normalize equation (30) using $\tau = t/T_d$ and $\xi = z(|\beta_2|/T_d^2)$. If we also use equation (29), we obtain

$$\frac{\partial A}{\partial \xi} + \frac{\mathrm{i}}{2}\frac{\partial^2 A}{\partial \tau^2} = \frac{\mathrm{i}C_x}{\tau_1^2} \sum_m \mathrm{sech}^2\left(\frac{\tau - m}{\tau_1}\right) A, \tag{31}$$

where we have introduced two normalized parameters as

$$C_x = \frac{2|\beta_{2s}|\omega_0}{\beta_2 \omega_s}, \qquad \tau_1 = \frac{T_s}{T_d}. \tag{32}$$

The parameter C_x governs XPM-induced coupling between the pump and probe pulses. Its value is close to 2 when $|\beta_{2s}|\omega_0 \approx \beta_2\omega_s$. The parameter τ_1 represents duty cycle of the train of pump pulses. Typically, τ_1 is $\sim$0.1 because the width of pump pulses should be a small fraction of their separation.

5.2. Momentum gaps

One can use equation (31) to find the band structure of a STBG created by pump pulses. This equation has the same mathematical form as the Schrödinger equation for an electron moving in a periodic potential, and one can use the Bloch theorem for solving it. Using $A(\xi,\tau) = \mathrm{e}^{\mathrm{i}\kappa\xi}B(\tau)$, we obtain the eigenvalue equation, $HB = \kappa B$, where the Hamiltonian has the form

$$H = -\frac{1}{2}\frac{\mathrm{d}^2}{\mathrm{d}\tau^2} + V(\tau), \tag{33}$$

and $V(\tau)$ is the periodic potential:

$$V(\tau) = \frac{C_x}{\tau_1^2} \sum_m \mathrm{sech}^2\left(\frac{\tau - m}{\tau_1}\right). \tag{34}$$

Notice that ξ plays the role of time and κ is the analog of energy is quantum mechanics.

From the Bloch theorem, $B(\tau)$ has the form $B(\tau) = \mathrm{e}^{-\mathrm{i}\Omega\tau}\bar{A}(\tau)$, where $\bar{A}(\tau)$ is a periodic function with the period τ_p of the soliton train ($\tau_p = 1$ in normalized units). We only need to solve equation (33) in the interval $[0, \tau_p]$. For given values of B and $B' = \mathrm{d}B/\mathrm{d}\tau$ at one end, one can solve the Schrödinger equation, $HB = \kappa B$, to find the values of B and B' at the other end in terms of a transfer matrix such that

$$\begin{pmatrix} B(\tau_p) \\ B'(\tau_p) \end{pmatrix} = M \begin{pmatrix} B(0) \\ B'(0) \end{pmatrix}, \tag{35}$$

where M denotes the transfer matrix. Its elements can be calculated by solving the Schrödinger equation two times with the initial conditions (i) $B = 1$, $B' = 0$ and (ii) $B = 0$, $B' = 1$. It is easy to show that $\exp(-\mathrm{i}\Omega\tau_p)$ is an eigenvalue of M. For a given value of κ, Ω may be real or complex. Solutions with real

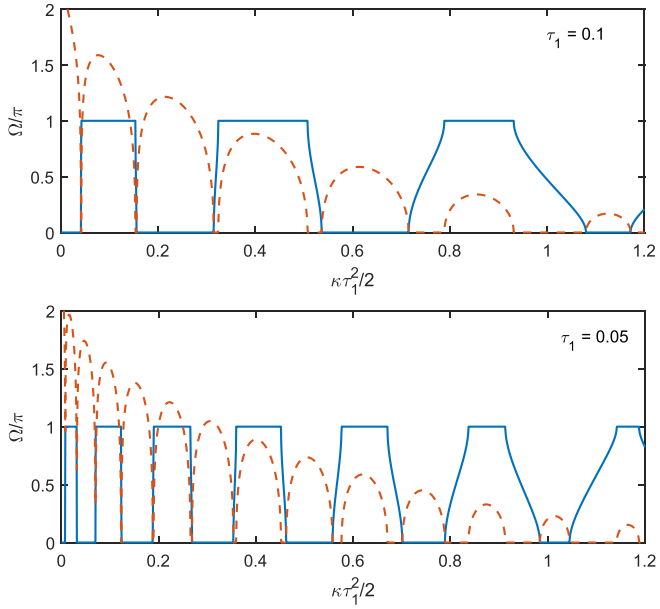

Figure 13. Band structure of a STBG for $\tau_1 = 0.1$ (top) or 0.05 (bottom). The real (solid line) and imaginary (dashed line) parts of Ω are plotted as a function of κ. Adapted with permission from [38] © The optical Society.

Ω correspond to propagating states, while those with complex Ω represent evanescent states.

The band structure of an STBG is found by calculating the frequency Ω as a function of κ. The real and imaginary parts of Ω are plotted in figure 13 as a function of κ for $\tau_1 = 0.1$ (top) and $\tau_1 = 0.05$ (bottom). The combination $\kappa\tau_1^2/2$ was used because its value of 1 corresponds to the barrier height produced by each soliton. As seen in figure 13, the real part of Ω vanishes in certain ranges of κ. These regions correspond to the momentum gaps in the moving frame used here.

Several features are noteworthy in figure 13. The number of momentum gaps depends on the value of τ_1 and increases as τ_1 is reduced. For a given value of τ_1, the width of gaps depends on the value of κ. The width of propagation bands is smaller for low values of κ. For larger values of κ, propagation bands become larger compared to the momentum gaps. This is because each soliton has a smaller reflectivity, and forming a band gap requires interference between multiple reflections.

5.3. Evolution of probe pulses

The evolution of a probe pulse has one limitation because it requires numerical solutions of equation (31). Whereas the band structure was calculated assuming that STBG is infinitely long with no ends, only a finite number of solitons can be used in numerical simulations. The first and last pulses act as temporal interfaces.

In a 2024 study [38], the soliton train contained 21 pulses, spaced such that $\tau_1 = 0.1$, and was confined to the region $-10 < \tau < 10$, marked by vertical dashed lines in figure 14, which shows the results obtained for a Gaussian probe pulse

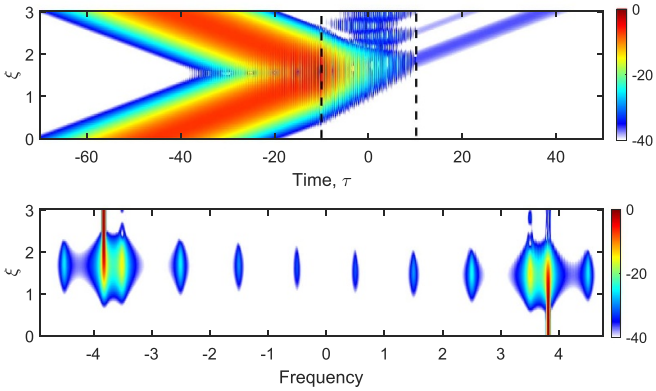

Figure 14. Total reflection of a probe pulse when κ falls inside a momentum gap of a STBG. Temporal (top) and spectral (bottom) evolution is shown along fiber's length. Adapted with permission from [38] © The optical Society.

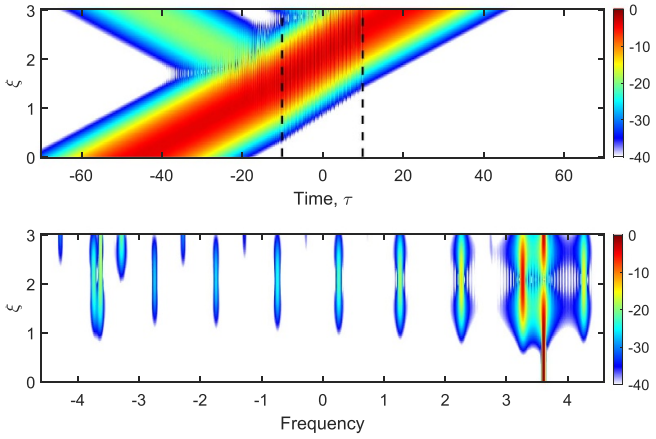

Figure 15. Same as figure 14 but κ is outside of a momentum gap, resulting in nearly total transmission of the probe pulse.

launched with the initial amplitude,

$$A(0,\tau) = \exp\left[-\frac{(\tau-\tau_s)^2}{2\tau_0^2} - i\Omega_i\tau\right], \qquad (36)$$

with $\tau_0 = 10$, $\tau_s = -45$, and $\Omega_i = 7.63\pi$. The bottom panel displays spectral evolution of this pulse.

As seen in figure 14, the probe pulse is initially far from the STBG formed by the soliton train. As it travels faster than pump pulses, it begins to interact with the grating at a distance $\xi = 1$ through the temporal interface located at $\tau = -10$. For the situation shown in figure 14, κ of the incident pulse, $\kappa_i = \Omega_i^2/2$, is determined by the dispersion relation of the homogeneous medium. For our choice of Ω_i, κ_i falls in the momentum gap of the STBG. This is the reason why probe pulse is almost totally reflected.

The probe pulse should be mostly transmitted through the STBG if its κ value falls outside of a momentum gap. Figure 15 shows this situation using the same parameter values, except for a small change in the input wavelength of the probe pulse ($\Omega_i = 7.23\pi$ in stead of 7.63π. As expected, probe pulse is mostly transmitted through the STBG. A small amount of

energy (about 3%) is reflected because of a mismatch between the modes propagating inside and outside of the grating region. Spectral evolution is also different in the two cases. Although multiple equally spaced side bands are generated in both cases, the probe's frequency undergoes a large spectral shift only in the total reflection case shown in figure 14. A much smaller spectral shift occurs when the probe is nearly transmitted through the STBG. However, its spectrum also contains several equally spaced side bands.

It is important to relate theoretical predictions to experiments and to discuss how an experiments can be designed to verify them. As we have seen, an STBG can be formed inside a silica fiber by launching a train of short pump pulses at a wavelength near 1550 nm. To suppress undesired higher-order nonlinear effects, one may choose $T_s = 1$ ps and $T_d = 10$ ps. In this case, STBG is formed by using 1.7 ps wide pump pulses separated by 10 ps. Using a realistic value of the GVD parameter, $\beta_2 = -20$ ps^2 km^{-1}, the normalized length $\xi = 1$ corresponds to 5 km. Thus, experiments will require several kilometers of fiber. The probe's wavelength should be chosen such that probe pulses travel at a speed close to that of pump pulses. One choice is 1145 nm in the normal-dispersion region of a silica fiber with its zero-dispersion wavelength near 1300 nm. Probe pulses should be considerably wider than pump pulses to interact with the grating. A value of $T_0 = 10$ ps for a Gaussian-shape probe corresponds to a full width at half maximum of 16.7 ps.

6. Photonic Anderson localization

So far, it has been assumed that an ideal train of pump pulses creates a STBG inside a silica fiber. In practice, pump pulses may not be equally spaced and their peak intensities mat not be the same because of pulse-to-pulse variations that can occur in any laser emitting short pulses. The question remains what happens when the solitons are not perfectly periodic inside the fiber.

Just as electrons can exhibit 'Anderson localization' in disordered crystals, a photonic analog of this concept has been found to occur for several optical devices [41–43]. In the context of optics, most past work has focused on transverse Anderson localization for which an optical beam exhibits localization in the plane transverse to the direction of propagation. In the case of a disordered STBG, it was found recently that localization occurs in the time domain, and it confines an optical pulse to its original time slot [38].

Disorder for an STBG can be created by randomizing variables such as each soliton's amplitude, width, or phase. An alternative is that all solitons in a train remain identical in all respects, and disorder is caused by random variations in their spacing. We focus on this later case. Mathematically, $\tau - m$ in equation (31) is replaced with $\tau - m - x_m$, where x_m varies in a random fashion with the integer m. In the 2024 study, a uniform distribution for x_m was employed in the interval $[-0.05, 0.05]$. Solving for the eigenstates of equation (31) for the choice $\tau_1 = 0.05$, it was found that a localized state exists when the STBG is not perfectly periodic. Figure 16 shows this

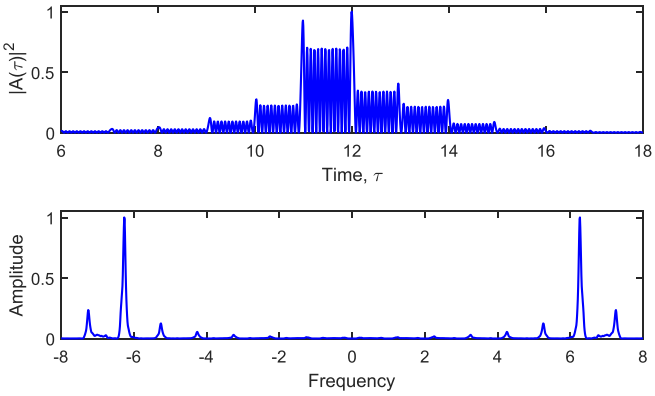

Figure 16. Localized eigenstate of a disordered STBG in the time (top) and frequency (bottom) domains. Adapted with permission from [38] © The optical Society.

eigenstate in the time domain (top), together with its spectrum (bottom). The value of κ for this state, $\kappa\tau_1^2/2 = 1.087$, lies in one of the propagation bands of a perfect Bragg grating (see figure 13).

The localized nature of the eigenstate in figure 16 is the result of the disorder in the soliton train induced by a nonuniform randomized pulse-to-pulse spacing. In the frequency domain, the spectrum of this eigenstate has two widely separated dominant peaks, which indicates that the localized state contains two waves propagating in the opposite directions (in the moving frame). Rapid oscillations in time are due to interference between two widely separated frequency components seen in the spectrum.

Numerical simulations were used in [38] to study how a localized state affect the evolution of a probe pulse. Since the localized mode in figure 16 consists of two widely separated frequency components, its excitation requires that the probe pulse to have a similar spectrum. This was ensured by taking the initial amplitude in the form

$$A(0,\tau) = \exp\left[-\frac{(\tau-\tau_s)^2}{2\tau_0^2}\right]\cos(\Omega_i\tau), \qquad (37)$$

with $\Omega_i = 12.5\pi$. The cosine term introduced rapid oscillations that produce a pulse shape similar to the localized mode shown in figure 16. Figure 17 compares the pulse's evolution in the disordered and perfect STBGs for $\tau_s = 11.7$ and $\tau_0 = 1.9$. The differences in the two cases are remarkable if we note that the disorder consisted of less that 5% fluctuations in the spacing of neighboring solitons.

In a disordered STBG, the probe pulse pulse remains localized at its initial position because of its coupling to the localized mode shown in figure 16. Only a small amount its energy radiates away because of a mismatch between the input pulse shape and the localized mode. When the disorder is not present, probe pulse excites two propagating modes of the crystal, traveling at different speeds and experiencing dispersion-induced broadening with propagation.

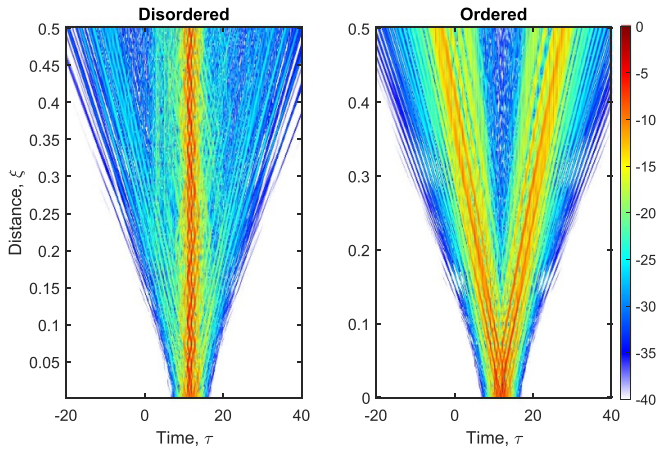

Figure 17. Evolution of a probe pulse in disordered and perfect STBGs, showing localization in the former case. Adapted with permission from [38] © The optical Society.

7. Concluding remarks

This review has focused on novel phenomena that emerge when optical pulses propagate through a spatiotemporal dispersive medium whose refractive index is modulated, both in space and time, in a traveling-wave fashion. Using optical fibers as an example of a dispersive medium, we first discussed the temporal analog of reflection at a moving index interface. A probe pulse incident at such a spatiotemporal interface splits into two parts with different optical spectra such that the reflected part never crosses the interface. When the index change is large enough, the temporal analog of TIR occurs, which allows one to construct temporal waveguides that confine pulses to within a time window of fixed duration.

The use of solitons through the Kerr effect shows how such novel effects can be observed in silica fibers by employing a pump-probe configuration. A single solitons acts as a time-domain mirror that can be used to produce large spectral shifts through temporal reflection. Two closely spaced solitons can be used to make a temporal waveguide that confines probe pulses through TIR between them. Two such solitons can also produce the temporal analog of a FPR by acting as partially reflecting mirrors. An even more exotic temporal structure, called the STBG here, can be created by launching a periodic train of pump pulses that travel as fundamental solitons inside an optical fiber. Such a device exhibits the so-called momentum gaps, resulting from temporal index variations that are periodic in nature. A probe pulse is mostly reflected from a STBG when the momentum of its photons lies inside of a momentum gap. A photonic analog of Anderson localization can also occur when disorder is introduced into a STBG.

We briefly comment on how a STBG differs from photonic time crystals that have attracted considerable attention recently [13, 16, 40]. The most striking feature of a photonic time crystal is the possibility of parametric amplification, possible because energy is not conserved in such a thermodynamically open system. Parametric amplification is not possible in the case of STBGs because the total number of photons is expected to be conserved in such a device.

Data availability statement

All data that support the findings of this study are included within the article (and any supplementary files).

Acknowledgments

The author is thankful to his collaborators, William Donaldson, Brent Plansinis, and Junchi Zhang, for working with him on the topics covered in this review. He also thanks Prof. Guy Millot for his hospitality at University of Burgundy, where this review was finalized. The financial support of the U.S. National Science Foundation is also acknowledged.

ORCID iD

Govind P Agrawal https://orcid.org/0000-0003-4486-8533

References

[1] Tournois P 1964 Analogie optique de la compression d'impulsion *C. R. Acad. Sci.* **258** 3839–42
[2] Akhmanov S A, Sukhorukov A P and Chirkin A S 1969 Nonstationary phenomena and space-time analogy in nonlinear optics *Sov. Phys. - JETP* **28** 748–57
[3] Salem R, Foster M A and Gaeta A L 2013 Application of space-time duality to ultrahigh-speed optical signal processing *Adv. Opt. Photon.* **5** 274–317
[4] Kolner B H 1994 Space-time duality and the theory of temporal imaging *IEEE J. Quantum Electron.* **30** 1951–63
[5] Goda K and Jalali B 2013 Dispersive Fourier transformation for fast continuous single-shot measurements *Nat. Photon.* **7** 102–12
[6] Mendonça J T and Shukla P K 2002 Time refraction and time reflection: two basic concepts *Phys. Scr.* **65** 160
[7] Xiao Y, Maywar D N and Agrawal G P 2014 Reflection and transmission of electromagnetic waves at a temporal boundary *Opt. Lett.* **39** 574–7
[8] Plansinis B W, Donaldson B W and Agrawal G P 2015 What is the temporal analog of reflection and refraction of optical beams? *Phys. Rev. Lett.* **115** 183901
[9] Gaafar M A, Baba T, Eich M and Petrov A Y 2019 Front-induced transitions *Nat. Photon.* **13** 737–48
[10] Caloz C and Deck-Léger Z 2019 Spacetime metamaterials—part I: general concepts *IEEE Trans. Antennas Propag.* **68** 1569–82
[11] Caloz C and Deck-Léger Z 2019 Spacetime metamaterials—part II: theory and applications *IEEE Trans. Antennas Propag.* **68** 1583–98
[12] Li H and Alù A 2021 Temporal switching to extend the bandwidth of thin absorbers *Optica* **8** 24–29
[13] Galiffi E, Tirole R, Yin S, Li H, Vezzoli S, Huidobro P A, Silveirinha M G, Sapienza R, Alù A and Pendry J B 2022 Photonics of time-varying media *Adv. Photon.* **4** 014002
[14] Boltasseva A, Shalaev V M and Segev M 2024 Photonic time crystals: from fundamental insights to novel applications: opinion *Opt. Mater. Express* **14** 592–7

[15] Morgenthaler F R 1958 Velocity modulation of electromagnetic waves *IRE Trans. Microwave Theory Tech.* **6** 167–72
[16] Sharabi Y, Dikopoltsev A, Lustig E, Lumer Y and Segev M 2022 Spatiotemporal photonic crystals *Optica* **9** 585–92
[17] Wang X, Mirmoosa M S, Asadchy V S, Rockstuhl C, Fan S and Tretyakov S A 2023 Metasurface-based realization of photonic time crystals *Sci. Adv.* **9** eadg7541
[18] Lustig E, Segal O, Saha S, Fruhling C, Shalaev V M, Boltasseva A and Segev M 2023 Photonic time-crystals—fundamental concepts *Opt. Express* **31** 9165–70
[19] Bacot V, Labousse M, Eddi A, Fink M and Fort E 2016 Time reversal and holography with spacetime transformations *Nat. Phys.* **12** 972–7
[20] Moussa H, Xu G, Yin S, Galiffi E, Ra'di Y and Alù A 2023 Observation of temporal reflection and broadband frequency translation at photonic time interfaces *Nat. Phys.* **19** 1–6
[21] Dong Z, Li H, Wan T, Liang Q, Yang Z and Yan B 2024 Quantum time reflection and refraction of ultracold atoms *Nat. Photon.* **18** 68–73
[22] Biancalana F, Amann A, Uskov A V and O'Reilly E P 2007 Dynamics of light propagation in spatiotemporal dielectric structures *Phys. Rev.* E **75** 046607
[23] Plansinis B W, Donaldson W R and Agrawal G P 2016 Temporal waveguides for optical pulses *J. Opt. Soc. Am.* B **33** 1112–9
[24] Plansinis B W, Donaldson W R and Agrawal G P 2018 Cross-phase-modulation-induced temporal reflection and waveguiding of optical pulses *J. Opt. Soc. Am.* B **35** 436–45
[25] Zhang J, Donaldson W R and Agrawal G P 2021 Temporal reflection and refraction of optical pulses inside a dispersive medium: an analytic approach *J. Opt. Soc. Am.* B **38** 997–1003
[26] Zhang J, Donaldson W R and Agrawal G P 2021 Impact of the boundary's sharpness on temporal reflection in dispersive media *Opt. Lett.* **46** 4053–6
[27] Agrawal G P 2019 *Nonlinear Fiber Optics* 6th edn (Academic)
[28] Philbin T G, Kuklewicz C, Robertson S, Hill S, König F and Leonhardt U 2008 Fiber-optical analog of the event horizon *Science* **319** 1367–70
[29] Demircan A, Amiranashvili S and Steinmeyer G 2011 Controlling light by light with an optical event horizon *Phys. Rev. Lett.* **106** 163901
[30] Tartara L 2012 Frequency shifting of femtosecond pulses by reflection at solitons *IEEE J. Quantum Electron.* **48** 1439–42
[31] Webb K E, Erkintalo M, Xu Y, Broderick N G R, Dudley J M, Genty G and Murdoch S G 2014 Nonlinear optics of fibre event horizons *Nat. Commun.* **5** 4969
[32] Goos F and Hänchen H 1947 Ein neuer und fundamentaler versuch zur totalreflexion *Ann. Phys., Lpz.* **436** 333–46
[33] Ponomarenko S A, Zhang J and Agrawal G P 2022 Goos-Hänchen shift at a temporal boundary *Phys. Rev.* A **106** L061501
[34] Boyd R W 2020 *Nonlinear Optics* 4th edn (Academic)
[35] Zhang J, Donaldson W R and Agrawal G P 2021 Time-domain Fabry–Perot resonators formed inside a dispersive medium *J. Opt. Soc. Am.* B **38** 2376–82
[36] Dudley J M, Genty G and Coen S 2010 *Fibre Supercontinuum Generation Overview* (Cambridge University Press) pp 52–61
[37] Wang S F, Mussot A, Conforti M, Zeng X L and Kudlinski A 2015 Bouncing of a dispersive wave in a solitonic cage *Opt. Lett.* **40** 3320–3
[38] Zhang J, Donaldson W R and Agrawal G P 2024 Spatiotemporal Bragg gratings forming inside a nonlinear dispersive medium *Opt. Lett.* **49** 5854–7
[39] Koufidis S F, Koutserimpas T T and McCall M W 2023 Temporal analog of Bragg gratings *Opt. Lett.* **48** 4500–3
[40] Asgari M M, Garg P, Wang X, Mirmoosa M S, Rockstuhl C and Asadchy V 2024 Theory and applications of photonic time crystals: a tutorial *Adv. Opt. Photon.* **16** 958–1063
[41] Segev M, Silberberg Y and Christodoulides D N 2013 Anderson localization of light *Nat. Photon.* **7** 197–204
[42] Mafi A 2015 Transverse Anderson localization of light: a tutorial *Adv. Opt. Photon.* **7** 459–515
[43] Yamilov A, Skipetrov S E, Hughes T W, Minkov M, Yu Z and Cao H 2023 Anderson localization of electromagnetic waves in three dimensions *Nat. Phys.* **19** 1308–13